Rigorous Treatment of Polytopal Rearrangements Reveal Surprising Complexity of Stereoisomerism Configuration Landscapes – Supplementary information

Peter J. Canfield*[a] and Maxwell J. Crossley*[a]

[a] School of Chemistry, The University of Sydney, NSW 2006, Australia

peter.canfield@sydney.edu.au,
maxwell.crossley@sydney.edu.au

Mathematica interactive tools for exploring the compactified S^2 AB_4 *T*-4 E-mode configuration space

Interactive Mathematica (v14.1) apps:

"any configuration in the AB4 T-4 E-mode configuration space.nb"

"great circles in the AB4 T-4 E-mode configuration space.nb"

Analytic expressions for the compactified S^2 AB_4 *T*-4 E-mode configuration space[1]

Using the Cartesian coordinates of the seed polytope $\mathbf{c_0}$:

$$\mathbf{c_0} = \begin{pmatrix} a & 0 & b \\ -a & 0 & b \\ 0 & a & -b \\ 0 & -a & -b \end{pmatrix}, \text{ where } a = \sqrt{\tfrac{2}{3}}\,, b = \sqrt{\tfrac{1}{3}}$$

and the two components of the E-mode normal mode (as angle-changing linear vectors relative to $\mathbf{c_0}$):

$$\boldsymbol{q_1} = \boldsymbol{\varepsilon}^1 = \tfrac{1}{2}\begin{pmatrix} 0 & 1 & 0 \\ 0 & -1 & 0 \\ 1 & 0 & 0 \\ -1 & 0 & 0 \end{pmatrix} \qquad \text{and} \qquad \boldsymbol{q_1} = \boldsymbol{\varepsilon}^2 = \begin{pmatrix} -b & 0 & a \\ b & 0 & a \\ 0 & -b & -a \\ 0 & b & -a \end{pmatrix}$$

the analytic expressions for all A–B^i unit vectors ($\mathbf{b}_i$) comprising the AB_4 *T*-4 E-mode configuration space $\bar{C}_{4E}$ are:

$$\bar{C}_{4E} = \begin{pmatrix} \mathbf{b}_1 \\ \mathbf{b}_2 \\ \mathbf{b}_3 \\ \mathbf{b}_4 \end{pmatrix} = \left\{ \begin{pmatrix} \frac{\sqrt{2}\cos\,\theta - \sin\,\phi_1 \sin\theta}{\sqrt{3}} & \cos\phi_1 \sin\theta & \frac{\cos\theta + \sqrt{2}\sin\,\phi_1 \sin\theta}{\sqrt{3}} \\ \frac{-\sqrt{2}\cos\theta + \sin\,\phi_1 \sin\theta}{\sqrt{3}} & -\cos\phi_1 \sin\theta & \frac{\cos\theta + \sqrt{2}\sin\,\phi_1 \sin\theta}{\sqrt{3}} \\ \cos\phi_1 \sin\theta & \frac{\sqrt{2}\cos\,\theta - \sin\,\phi_1 \sin\theta}{\sqrt{3}} & \frac{-\cos\theta + \sqrt{2}\sin\,\phi_1 \sin\theta}{\sqrt{3}} \\ -\cos\phi_1 \sin\theta & \frac{-\sqrt{2}\cos\theta + \sin\,\phi_1 \sin\theta}{\sqrt{3}} & \frac{-\cos\theta + \sqrt{2}\sin\,\phi_1 \sin\theta}{\sqrt{3}} \end{pmatrix} \middle| \; \theta \in [0,\pi), \phi \in [0,2\pi) \right\}$$

Examples of polytope configurations and absolute configurations.

Tetrahedral tetracoordinate
Genus: *T*-4
Generic symmetry: T_d
Species: *T*-4-*R*
Specific symmetry: C_1

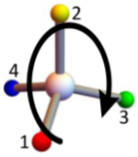

Tetragonally compressed tetrahedral tetracoordinate
Genus: *TCT*-4
Generic symmetry: D_{2d}
Species: *TCT*-4-4-*S*
Specific symmetry: C_1

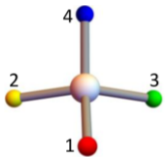

Tetragonally elongated tetrahedral tetracoordinate
Genus: *TET*-4
Generic symmetry: D_{2d}
Species: *TET*-4-4-*S*
Specific symmetry: C_1

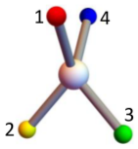

Twisted tetrahedral tetracoordinate
Genus: *TT*-4
Generic symmetry: D_2
Species: *TT*-4-*R*
Specific symmetry: C_1

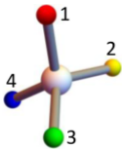

Square planar tetracoordinate
Genus: *SP*-4
Generic symmetry: D_{4h}
Species: *SP*-4-4
Specific symmetry: C_s

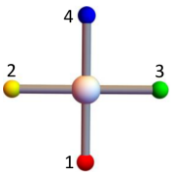

Gyfu planar tetracoordinate
Genus: *GYP*-4
Generic symmetry: D_{2h}
Species: *GYP*-4-3-2
Specific symmetry: C_s

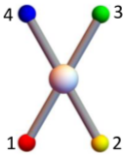

Symmetric linear tetracoordinate
Genus: *SL*-4
Generic symmetry: $D_{\infty h}$
Species: *SL*-4-2
Specific symmetry: $C_{\infty v}$

Graph symmetries of the compactified S^2 AB_4 *T*-4 E-mode configuration space

a) View centred on a *SL*-4 polytope graph vertex (1 of 6 graph C_4 axes)

b) View centred on a *T*-4 polytope graph vertex (1 of 8 graph C_3 axes)

c) View centred on a *SP*-4 polytope graph vertex (1 of 12 graph C_2 axes)

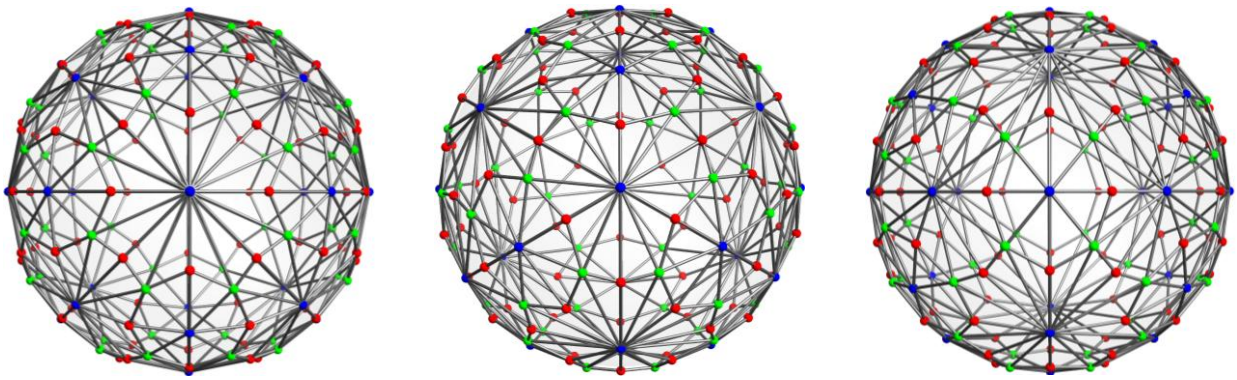

Blue vertices: *SL*-4, *T*-4, and *SP*-4 species; red vertices: *TCT*-4, *TET*-4, and *GYP*-4 species; green vertices: *TT*-4 species

Fig. S1 3D perspective renderings of the AB_4 *T*-4 E-mode undirected simple graph illustrating configuration space symmetries. a) View along a graph C_4 axis with *SL*-4-2 polytope graph vertex centred. b) View along a graph C_3 axis with *T*-4 polytope graph vertex centred. c) View along a graph C_2 axis with *SP*-4 polytope graph vertex centred.

Example great circle S^1 configuration subspaces of the full compactified S^2 AB_4 *T*-4 E-mode configuration space

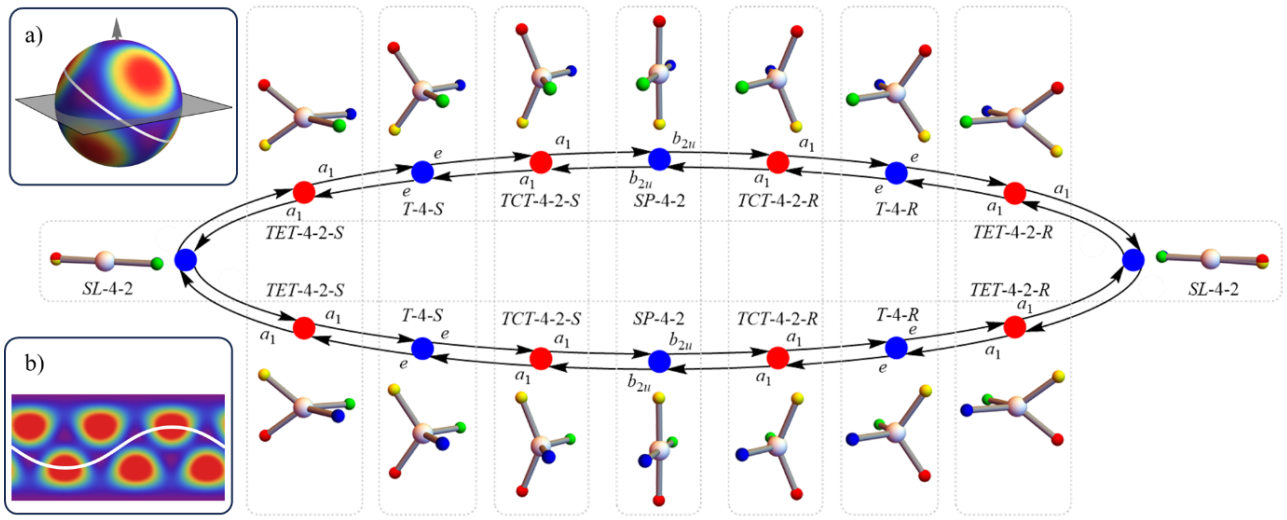

Fig. S2 (Equivalent to Figure 9 in the main text.) One-dimensional great circle polytopal rearrangement configuration-space ring and orientation permutation pseudorotations. Polytopal rearrangements arise from antisymmetric orthogonal paired bond-angle flexions of *T*-4 configurations. Pairs of orientation permutation are indicated in dotted grey enclosures. This trajectory corresponds to the white track shown in the full AB_4 *T*-4 E-mode space (inset a) and its equirectangular projection (inset b). B-atoms are distinctly coloured for tracking purposes.

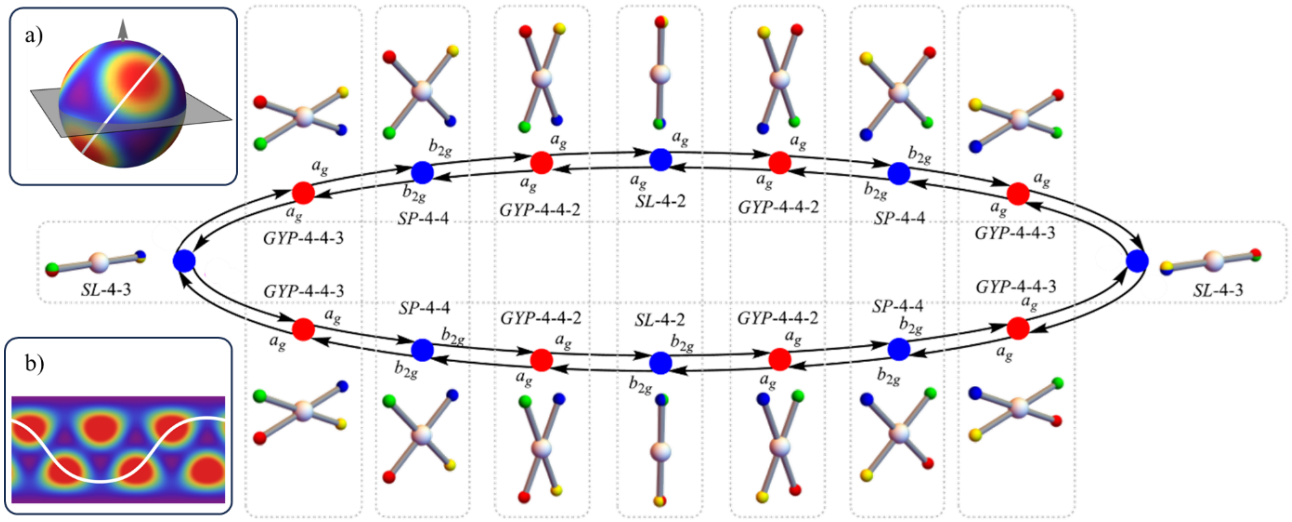

Fig. S3 One-dimensional great circle polytopal rearrangement configuration-space ring and orientation permutation pseudorotations arising from antisymmetric coplanar paired bond-angle flexions of the *SP*-4-4 configuration. The space is composed of pairs of orientation permutated *SL*-4-2 and *SL*-4-3 species, and four orientation permuted *SP*-4-4, *GYP*-4-4-2, and *GYP*-4-4-3 species (dotted grey enclosures). This trajectory corresponds to the white track shown in the full AB_4 *T*-4 E-mode space (inset a) and equirectangular projection (inset b). B-atoms are distinctly coloured for tracking purposes.

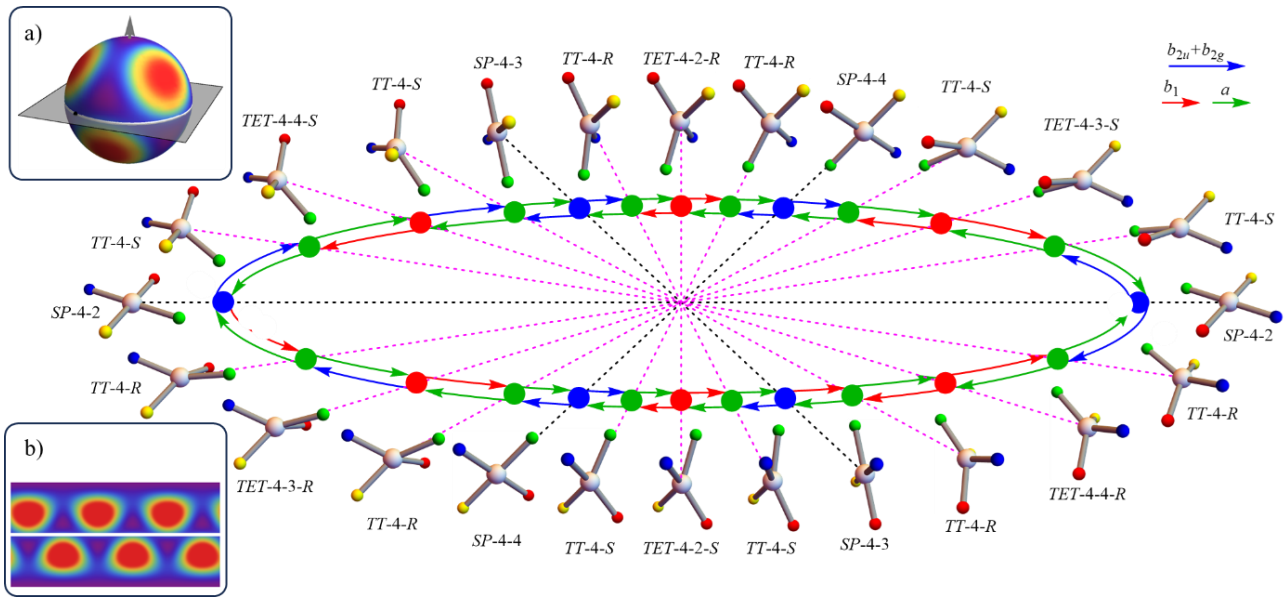

Fig. S3 One-dimensional great circle polytopal rearrangement configuration-space ring and orientation permutation pseudorotations corresponding to the white equatorial track shown in the full AB_4 *T*-4 E-mode space (inset a) and its equirectangular projection (inset b). Enantiomers are indicated by dashed magenta lines. Orientation permuted achiral pairs are indicated by the black dashed lines. Generic symmetries transforming action (directed graph edges) are colour coded and shown in the upper right corner. B-atoms are distinctly coloured for tracking purposes.

Method for potential energy surfaces

Qualitative PESs were generated using modest-level density-functional theory (DFT) calculations performed with Gaussian16[2] at the B3LYP-D3BJ level[3-5] using the inbuilt 6-31G* basis set for H, F, Si, Cl, along with the SDD basis set and pseudopotential for I and Xe. For the bond-length restricted calculations, each A–B^i bond was set to that of a calculated local-minimum structure. Geometries involving chemically unrealistic close B^i – B^j distances were omitted from the calculations. For the bond-length relaxed calculations on tetrafluorides, initial bond lengths were set as either the local-minimum values or scaled to approximate dissociation as F_2 units. For the chiral silane example, all starting geometries used local-minimum bond length values. Some relaxed geometries in the vicinity of the "fusion" structures proved problematic so conventional D_2 symmetry constrained potential energy scans based upon the B^1–A–B^2 angle and the digonal twist angle (see below) were performed. The resulting fine-grained potential energy surface regions were then scaled, rotated, and fitted in place to amend the corresponding region of the configuration space.

Gaussian16[2] script for D_2-symmetry constrained potential energy surface scan

```
#P b3lyp/gen pseudo=read empiricaldispersion=gd3bj symm=(veryloose,follow) integral=ultrafinegrid opt=(z-matrix,maxstep=9)
scf=(save,intrep)

SL-4_region_scan

0 1
Xe
Bq  1 3.
F   1 bond  2 ang
F   1 bond  2  ang  3 lin
Bq  1 3. 2 ra 3 zero
Bq  1 3. 5 ra 2 -lin
F   1 bond  6 ang  5 twist
F   1 bond  6 ang  7 -lin
  Variables:
bond 2.12
ang 40.
twist 90. S 9 -10.
  Constants:
ra 90.
lin 180.
zero 0.

F 0
6-31g*
****
Xe 0
SDD
****

Xe 0
SDD
```

References

1. P. J. Canfield, M. J. Crossley, J. Spreer and S. Tillmann, *ChemRxiv*, 2025, DOI: 10.26434/chemrxiv-2025-gc7s6.
2. M. J. Frisch, G. W. Trucks, H. B. Schlegel, G. E. Scuseria, M. A. Robb, J. R. Cheeseman, G. Scalmani, V. Barone, G. A. Petersson, H. Nakatsuji, X. Li, M. Caricato, A. V. Marenich, J. Bloino, B. G. Janesko, R. Gomperts, B. Mennucci, H. P. Hratchian, J. V. Ortiz, A. F. Izmaylov, J. L. Sonnenberg, Williams, F. Ding, F. Lipparini, F. Egidi, J. Goings, B. Peng, A. Petrone, T. Henderson, D. Ranasinghe, V. G. Zakrzewski, J. Gao, N. Rega, G. Zheng, W. Liang, M. Hada, M. Ehara, K. Toyota, R. Fukuda, J. Hasegawa, M. Ishida, T. Nakajima, Y. Honda, O. Kitao, H. Nakai, T. Vreven, K. Throssell, J. A. Montgomery Jr., J. E. Peralta, F. Ogliaro, M. J. Bearpark, J. J. Heyd, E. N. Brothers, K. N. Kudin, V. N. Staroverov, T. A. Keith, R. Kobayashi, J. Normand, K. Raghavachari, A. P. Rendell, J. C. Burant, S. S. Iyengar, J. Tomasi, M. Cossi, J. M. Millam, M. Klene, C. Adamo, R. Cammi, J. W. Ochterski, R. L. Martin, K. Morokuma, O. Farkas, J. B. Foresman and D. J. Fox, *Gaussian 16 Rev. C.01*, Wallingford, CT, 2016.
3. A. D. Becke, *J. Chem. Phys.*, 1993, **98**, 5648-5652.
4. C. Lee, W. Yang and R. G. Parr, *Phys. Rev. B*, 1988, **37**, 785.
5. S. Grimme, S. Ehrlich and L. Goerigk, *J. Comput. Chem*, 2011, **32**, 1456-1465.